JSHC
Japan Society of
Histochemistry and Cytochemistry
Established 1959

Acta Histochem. Cytochem. 47 (6): 273–288, 2014
doi: 10.1267/ahc.14038

Immuno- and Enzyme-histochemistry of HRP for Demonstration of Blood Vessel Permeability in Mouse Thymic Tissues by "*In Vivo* Cryotechnique"

Bao Wu[1], Nobuhiko Ohno[1], Yurika Saitoh[1], Yuqin Bai[1], Zheng Huang[1], Nobuo Terada[1] and Shinichi Ohno[1]

[1]*Department of Anatomy and Molecular Histology, Interdisciplinary Graduate School of Medicine and Engineering, University of Yamanashi, 1110 Shimokato, Chuo-City, Yamanashi 409–3898, Japan*

Received July 3, 2014; accepted September 29, 2014; published online November 21, 2014

It is difficult to understand the *in vivo* permeability of thymic blood vessels, but "*in vivo* cryotechnique" (IVCT) is useful to capture dynamic blood flow conditions. We injected various concentrations of horseradish peroxidase (HRP) with or without quantum dots into anesthetized mice via left ventricles to examine architectures of thymic blood vessels and their permeability at different time intervals. At 30 sec after HRP (100 mg/ml) injection, enzyme reaction products were weakly detected in interstitium around some thick blood vessels of corticomedullary boundary areas, but within capillaries of cortical areas. At 1 and 3 min, they were more widely detected in interstitium around all thick blood vessels of the boundary areas. At 10 min, they were diffusely detected throughout interstitium of cortical areas, and more densely seen in medullary areas. At 15 min, however, they were uniformly detected throughout interstitium outside blood vessels. At 30 min, phagocytosis of HRP by macrophages was scattered throughout the interstitium, which was accompanied by decrease of HRP reaction intensity in interstitial matrices. Thus, time-dependent HRP distributions in living mice indicate that molecular permeability and diffusion depend on different areas of thymic tissues, resulting from topographic variations of local interstitial flow starting from corticomedullary areas.

Key words: mouse thymus, *in vivo* cryotechnique, HRP, immunolocalization, enzyme-histochemistry

I. Introduction

The living animal thymus is one of the lymphoid organs, where lymphocyte precursors undergo complex processes of cellular maturation, resulting in translocation of mature thymocytes to peripheral lymphoid organs [18, 19, 28]; however, it is still unclear whether the selection of thymocytes depends on the direct entrance of extrinsic soluble molecules from blood vessels into the thymus. The transport mechanism of such soluble molecules throughout the interstitial matrix of thymic tissues has been assumed to be closely associated with blood circulation conditions *in vivo*. Therefore, thymocyte behavior depends on the complex interstitium and microenvironments, which influence the transport of fluid and soluble molecules from blood vessels. Previously, the flow system of such molecules into the thymic interstitial matrices was examined by artificial injection of horseradish peroxidase (HRP) into blood vessels [29]. As the injected HRP was found to be mainly localized in the interstitium of the corticomedullary boundary and medulla, the concept of the "blood-thymus barrier" was proposed, which had been postulated in the previous decade [21]. Other researchers, however, doubted the validity of its concept, because of the existence of some injected bovine serum albumin (BSA) in the thymic cortex [31], and also little ultrastructural evidence of completely

Correspondence to: Shinichi Ohno, M.D., Ph.D., Professor and Chairman, Department of Anatomy and Molecular Histology, Interdisciplinary Graduate School of Medicine and Engineering, University of Yamanashi, 1110 Shimokato, Chuo-city, Yamanashi 409–3898, Japan.
E-mail: sohno@yamanashi.ac.jp

sealing features of blood vessel walls [8, 11]. In those reports, ultrastructural findings of the histological architecture and immunolocalization of extrinsic soluble proteins were obtained in thymic tissue specimens prepared by conventional chemical fixation, which is well known to cause technical artifacts, such as tissue shrinkage and the extraction or diffusion of soluble proteins [9, 10, 22]. This morphofunctional discrepancy in thymic tissues should be re-examined *in vivo* by injecting HRP into living mice. Thus, it was difficult to conclude the precise immunolocalization of soluble proteins in thymic tissues with conventional immersion- or perfusion-fixation due to their diffusion artifacts. Therefore, the definite immunolocalization of soluble HRP proteins with small molecular weight should be reconfirmed in the whole interstitium of thymic tissues *in vivo* of living mice.

In the previous study, our "*in vivo* cryotechnique" (IVCT) was performed for the living mouse thymus to reveal the immunolocalization of intrinsic mouse serum proteins or extrinsic BSA injected via tail veins [3]. As already discussed in detail [1, 2, 25, 26], any target organs of living animals could be directly frozen without artificial tissue resection or conventional perfusion-fixation by the IVCT, which captured the molecular localization of cells and tissues without technical artifacts [33]. In particular, IVCT-prepared tissue specimens efficiently retained soluble intrinsic or extrinsic proteins *in situ*, in combination with the common freeze-substitution (FS) fixation [33]. Therefore, the immunolocalization of such proteins *in vivo* could be directly re-examined in paraffin-embedded tissue sections, as already reported [24, 32–35].

Early permeability studies of thymic blood vessels suggested the existence of the blood-thymus barrier [21, 29], allowing the passage of low molecular weight tracers, while mostly excluding high molecular weight particles. In the past few years, we have demonstrated the immunolocalization of mouse original albumin, immunoglobulin G1 (IgG1), IgA, and IgM in living mouse thymus, as well as intravenously injected BSA [3]. In the previous report [3], time-dependent penetration of circulating BSA into the living mouse thymus and its distribution in the thymic parenchyma might be not only governed by the permeability properties of vascular walls, but also by the spatial architecture of blood vessels within thymic lobules. The outer cortex of lobules is known to be mainly supplied by blood capillaries with small diameters, whereas the inner cortical areas near the medulla contain thick blood vessels of varying sizes, the largest being efferent limbs of the blood vessel loops, as schematically summarized in Figure 2b. As mentioned before [3], the IVCT revealed the definite immunolocalization of mouse serum albumin and IgG1, in addition to extrinsic BSA, in the local interstitium of living mouse thymic tissues, indicating the different accessibility of mouse serum proteins from corticomedullary boundary areas.

Common HRP with a smaller molecular weight of about 40,000 is known to have constant high enzyme reactivity with a small specific substrate, such as hydrogen peroxide, which was famously used for HRP localization of kidney tissues, showing its reabsorption mechanism of epithelial cells in convoluted proximal tubules [6], in addition to thymic organs [29]. Therefore, we used the similar enzymological protocol of cryosections for translocation of HRP leaking through thymic blood vessel walls, and then performed double-fluorescence immunostaining for other proteins in paraffin sections. It would be interesting for us to consider whether the distribution of HRP protein throughout the interstitial matrices depends on the time interval after its injection and its concentration. In the present study, we also tried to identify the immunolocalization of extrinsic HRP in living mouse thymic tissues, which were directly injected via left ventricles, at short time intervals of second or minute orders by the IVCT-FS, and to reveal some morphofunctional features of the dynamically changing barriers of the thymic tissues. Our final goal was to clarify how thymic complex tissues affected the time-dependent distribution of injected smaller antigenic proteins of various concentrations, probably resulting in immunological reactions.

II. Materials and Methods

Injection of horseradish peroxidase (HRP) or quantum dots (QDs)

The present study was performed in accordance with the guidelines governing animal experiments at the University of Yamanashi. Male C57BL/6J mice, aged 6–8 weeks, were anesthetized with sodium pentobarbital (50 mg/kg body weight), and surgically treated to expose their trachea, which was immediately connected to an artificial respiratory ventilator, as reported before [3]. Their thoracic cavities were carefully opened to expose thymic tissues (Fig. 1a). Then, 50 µl HRP (Type II; Sigma-Aldrich, St. Louis, MO, USA/MW; 40,000, size; 25–30 Å) at concentrations of 10, 25, 50, 100 mg/ml (Fig. 1b, c, d) was continuously injected into the left ventricles of beating hearts through 30-gauge needles at a constant flow speed of 10 µl/s, as reported previously [36], because the blood volume in the left ventricle of a normal mouse heart is reported to be 350–400 µl/s (70–80 µl/beat × 5 beats/s) [14]. At 30 sec, 1, 3, 10, 15 and 30 min (Fig. 1g, h) after starting the continuous HRP injection, liquid isopentane-propane mixture (−193°C) pre-cooled in liquid nitrogen was directly poured over the thymic tissues, as reported previously [3].

For some mice, 50 µl of 45 µM glutathione (GSH)-quantum dots (QDs) was similarly injected into their left ventricles (Fig. 1e) [36], and then the IVCT was performed in a similar way on their thymus at 3, 10, 15 and 30 sec (Fig. 1j, h) after the QDs injection, as described above. The final concentration of the injected QDs was calculated to be about 35–40 times diluted, resulting in about 1.2 µM in blood concentration, as reported previously [36]. Then, liq-

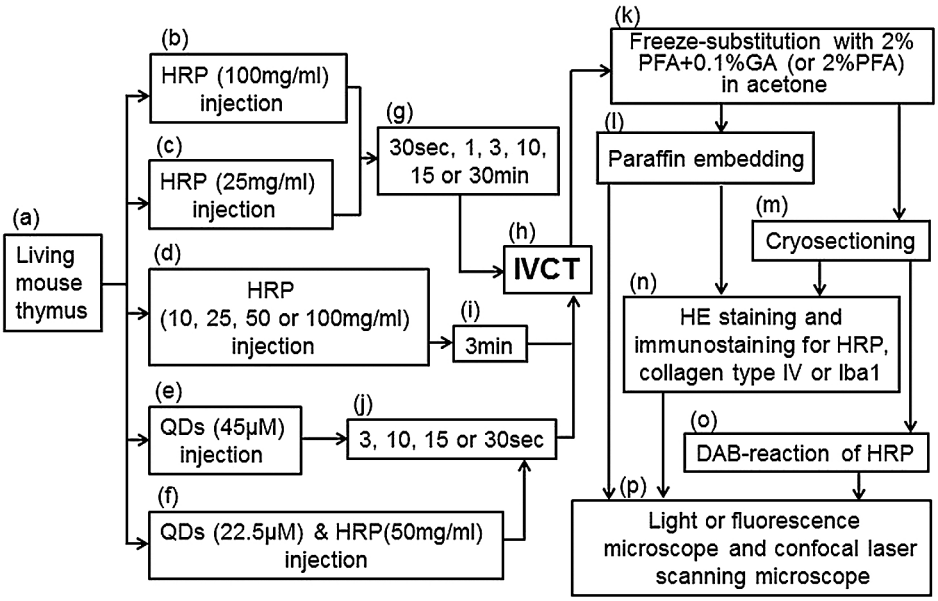

Fig. 1. A flow chart of five different treatments (**b–f**) of the living mouse thymus (**a**). Various concentrations of HRP (**b, c, d, f**) or QDs (**e, f**) were injected through left ventricles of living mice, which were prepared various time intervals (**g, i, j**) after their injections by IVCT (**h**). (**k–p**) A series of preparation steps for observation of thymic tissues by microscopy.

uid nitrogen was additionally used to maintain the frozen thymic organs at a low temperature of –196°C. They were trimmed with a pair of nippers and also a dental electric drill in liquid nitrogen, and then processed for the common freeze-substitution step, as described below. The QDs used in this study, referred to as GSH-QD650, were made of a CdSe/CdZnS core with glutathione (GSH) coating, and were about 8 nm in total diameter, emitting red (around 650 nm in wavelength) fluorescent signals with ultraviolet (UV) light, as already described in detail [12, 37].

For other mice, 50 μl of both 22.5 μM QDs and HRP at a concentration of 100 mg/ml was continuously injected at a constant speed of 10 μl/sec into left ventricles of beating hearts, as described above. Then the IVCT was performed on their thymus in a similar way at 3, 10, 15 and 30 sec after the QD and HRP injection (Fig. 1f, j, h).

Freeze-substitution (FS) fixation and subsequent tissue preparations

The routine FS solution consisted of absolute acetone containing 2% paraformaldehyde (PFA) alone or a mixture of 2% PFA and 0.1% glutaraldehyde (GA) (Fig. 1k), which was prepared using a molecular sieve (Type 3A; Nacalai Tesque Inc., Kyoto, Japan), as reported previously [32]. The frozen thymic tissues were kept at about –80°C in FS solution for 24 hr. They were then put into a deep freezer at –20°C for 2 hr, and finally into a refrigerator at 4°C for 2 hr. Subsequently, some tissue specimens were washed in pure acetone, infiltrated with xylene at room temperature, and routinely embedded in paraffin wax (Fig. 1l). The paraffin-embedded specimens were cut into 4 μm slices and mounted on glass slides.

Enzyme-histochemistry of injected HRP in thymic tissues

For observation of other HRP-injected thymic tissues, the IVCT-frozen specimens were first processed to the FS step for fixation, as described above. In the case of enzyme-histochemistry, the FS solution consisted of absolute acetone containing a mixture of 2% PFA and 0.1% GA. The temperature of the frozen specimens was gradually increased, as described in the previous paragraph. Subsequently, they were infiltrated with 30% sucrose and 5% glycerol in phosphate-buffered saline (PBS), pH 7.4, and frozen with isopentane solution precooled in dry ice. The frozen tissues were cut into 8 μm slices and mounted on MAS-coated glass slides (Matsunami Glass Co. Ltd, Osaka, Japan) (Fig. 1m). After washing in PBS, they were treated with metal-enhanced diaminobenzidine (DAB) solution (Thermo Fisher Scientific Inc., Rockford, IL, USA) for 1 min (Fig. 1o), were later treated with 0.05% osmium tetroxide, as reported previously [32, 34], and observed under a bright-field light microscope (Fig. 1p). The HRP permeability grades of vascular walls were semi-quantitatively assessed by calculating the number of vessels with HRP-positive interstitial parts per outer cortical or corticomedullary area of tissue sections at various time intervals after the HRP injection. Serial sections were routinely stained with methyl green for visualizing nuclei to discriminate between thymic compact cortex and loose medulla areas.

Fluorescent QD observation in thymic tissues

The QD-injected thymic tissues were de-paraffinized and directly mounted on glass slides with Multi Mount 220 (Matsunami Glass Co. Ltd) to visualize QDs without any staining by fluorescence microscopy, as reported previously (Fig. 1p) [36].

Immunohistochemical analyses for HRP and Iba1

Paraffin-embedded tissue sections of 4 μm thickness were mounted on MAS-coated glass slides, and some were routinely deparaffinized for hematoxylin and eosin (HE) staining (Fig. 1n). The other deparaffinized sections were rehydrated in PBS and immunostained with goat affinity-purified anti-HRP antibody (Jackson Immunoresearch, Baltimore, PA, USA) or rabbit anti-Iba1 antibody (Wako, Richmond, VA, USA) (Fig. 1n). Briefly, serial tissue sections for immunoperoxidase staining were first blocked with 1% hydrogen peroxide in PBS and incubated in PBS containing 5% fish gelatin (Sigma, St. Louis, MO, USA) for 1 hr. They were then treated with each antibody in PBS containing 5% fish gelatin at 4°C overnight. The immunostained sections were additionally incubated with biotin-conjugated rabbit polyclonal anti-goat IgG antibody or biotin-conjugated goat polyclonal anti-rabbit IgG antibody (Vector, Burlingame, CA, USA) at room temperature for 1 hr. The immunoreaction products were visualized with the avidin–biotin–HRP complex (ABC) method (Vector) and a DAB substrate kit (Pierce, Rockford, IL, USA), and additionally fixed with 0.05% osmium tetroxide solution, as reported previously [32, 34]. All immunostained sections were counterstained with methyl green, and finally observed with a light microscope (BX-61; Olympus, Tokyo, Japan) (Fig. 1p).

Double-immunofluorescence staining for HRP and collagen type IV

Some deparaffinized tissue sections were blocked with 5% fish gelatin in PBS for 1 hr and treated with rabbit anti-HRP and goat anti-collagen type IV polyclonal antibodies at 4°C overnight (Fig. 1n). Then, they were incubated with Alexa Fluor 488-conjugated donkey anti-rabbit IgG antibody and Alexa Fluor 594-conjugated donkey anti-goat IgG antibody (Life Technologies, Eugene, OR, USA) at room temperature for 1 hr. Finally, intracellular nuclei were counterstained with 4,6-diamidino-2-phenylidole (DAPI), and the immunostained sections were mounted on glass slides with Vectashield (Vector) and observed under a confocal laser scanning microscope (FV-1000; Olympus) (Fig. 1p).

III. Results

Morphological findings of living mouse thymic tissues

By HE staining, two common zones were seen in the thymic tissues, namely both the peripheral cortex (Fig. 2a–d, f, g) and central medulla (Fig. 2a–c, e). Extracellular spaces of the thymic interstitum with open blood vessels were well maintained in the specimens prepared by the IVCT method (Fig. 2c–g) because the interstitial tissues shrank much less during the preparation steps in comparison with the conventional preparation methods, as described previously [3]. An increase or decrease in the cortex/medulla ratio was variously seen, depending on the cutting plane of tissue sections within each lobule, which were carefully checked in these HE-stained sections. A normal cortex/medulla ratio of thymic tissues would be close to 2:1 in a typical adult rodent, as already reported [5]. When considering vascular patterns of the thymus in relation to its functional role, as schematically summarized in Figure 2b, attension should be paid to blood capillaries in the cortex and also to large venules in the medulla. Interlobular arteries usually reached the medullary parenchyma at the end of septa and immediately branched into smaller arteries or arterioles (Fig. 2b, c). Briefly, the thymic cortex consisted of compact thymocytes along with a fine network of open blood capillaries *in vivo* (Fig. 2c, g), and corticomedullary boundary areas were also characterized by blood vessels containing many flowing erythrocytes (Fig. 2c, f). Most blood vessels in the cortex were blood capillaries (Fig. 2c, d, g), and thicker arterioles with diameters of 15–30 μm were found in the corticomedullary boundary areas (Fig. 2c, f). Those arterioles ran outwards into blood capillary branches in the deep cortex (Fig. 2b, c, g). The cortical blood capillaries were directed almost radially (Fig. 2a–c), and made a coarse and anastomosing network. Smaller capillaries lay beneath the capsule (Fig. 2d). Large and medium lymphocytes, which were actively proliferating, were most numerous in the cortex (Fig. 2d, g). In contrast, the thymic medulla showed much paler HE staining intensity with large reticulum cells (Fig. 2c, e, f), because of the much lower cellularity of thymocytes (Fig. 2e). Postcapillary venule diameters were seen to widely range from 15 to 50 μm in the medulla and in the corticomedullary boundary areas (Fig. 2c, e, f). Large epithelial reticulum cells were observed in all areas of the cortex, corticomedullary boundary, and medulla (Fig. 2c–g).

Enzyme-histochemistry of injected HRP in cryosections of thymic tissues

Enzyme-reactive intensities of HRP with methyl green (MG) staining were detected at various time intervals in cryosections of mouse thymic tissues (Fig. 3), which were injected with HRP (100 mg/ml) via left ventricles. The DAB reactivity of HRP with high sensitivity was not found in the interstitium of the cortex without HRP injection (Fig. 3a, b). However, flowing erythrocytes in blood vessels were usually positive for the DAB reaction in cryosections, because of their usual endogenous peroxidase activity. Enzyme reaction products of injected HRP protein were serially localized not only in blood vessels, but also in the interstitial matrices of the thymic cortex of living mice. At 30 sec after the HRP injection, enzyme reaction products were slightly detected in the interstitium around some thick blood vessels (Fig. 3c), probably arterioles in corticomedullary boundary areas in addition to venules in the medulla and also within blood capillaries of the cortex (Fig. 3d). Fine cortical vessels have diameters of 4–8 μm in largest dimension, as already shown in Figure 2g. Larger blood vessels were near the medulla (Fig. 3c, d). The intense

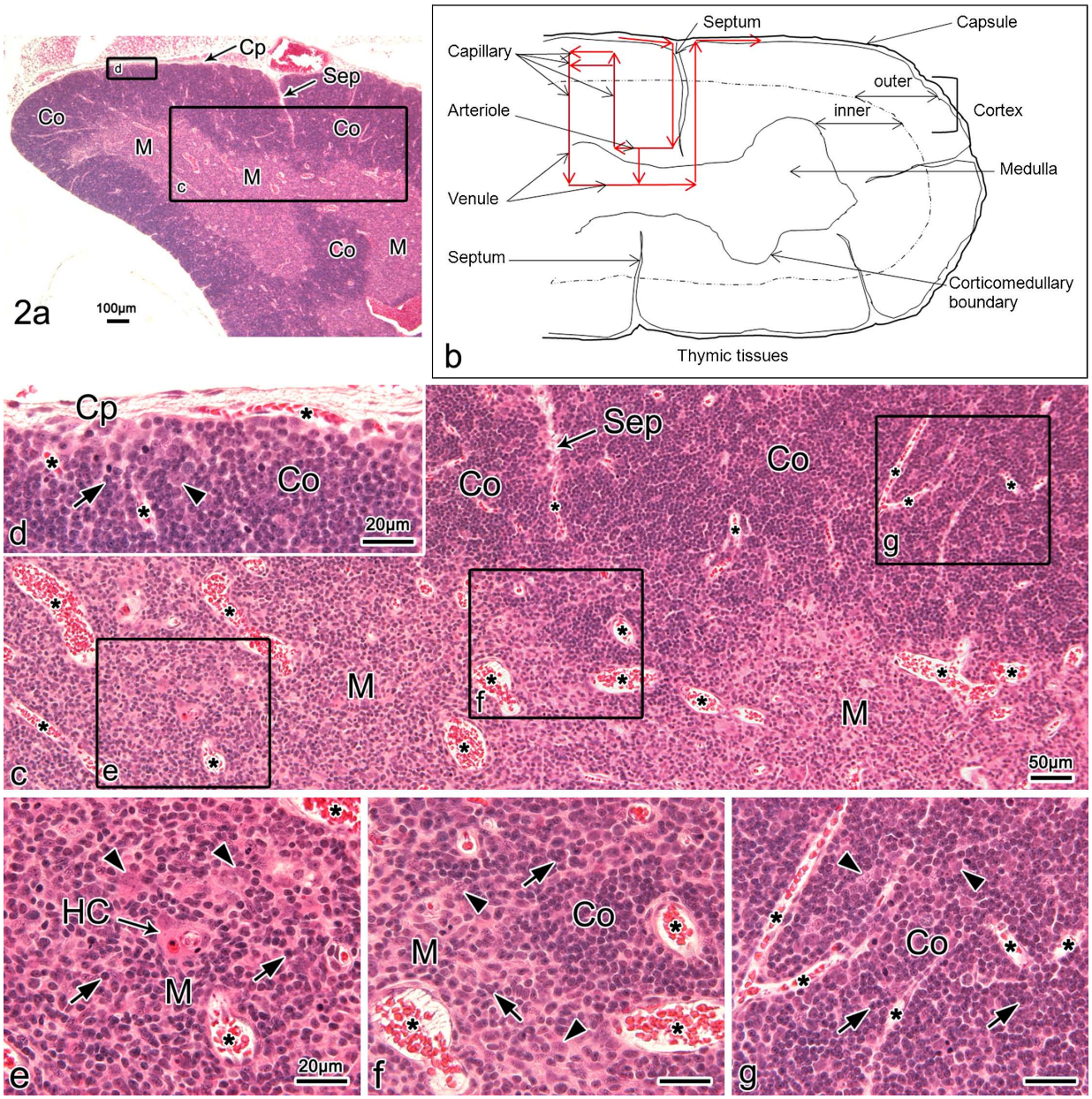

Fig. 2. Light micrographs of hematoxylin-eosin staining of paraffin sections of living mouse thymic tissues prepared by IVCT (**a, c–g**) and schematic representation of blood vessel routes (**b**) as already described. (**a**) A low-magnification view of the thymic tissues shows widely panoramic tissue areas, extending from the superficial cortex (Co) under the capsule (Cp) to the deep medulla (M). (**b**) As previously reported, the blood vessel route schematically shows an anastomosing network in the cortex, and the cortical capillaries merge into venules in the medulla, which return to the septum and capsule. (**c–g**) Each micrograph is a highly magnified view of the area enclosed with each rectangle in **a** and **c**. (**c**) Many small thymocytes, large epithelial reticulum cells, and open blood vessels (asterisks) with flowing erythrocytes are detected in the areas of the cortex (Co) and medulla (M). (**d**) Cortical blood capillaries with erythrocytes (asterisks) are seen in the subcapsular region in addition to capsular blood capillaries (asterisks). (**e**) Medulla (M) is composed of fewer thymocytes (arrows) and epithelial reticulum cells (arrowheads), and a Hassall's corpuscle (HC) is also seen. (**f**) Corticomedullary boundary areas contain thick blood vessels (asterisks), extending into both cortical (Co) and medullary (M) areas. Their opening lumen is well delineated endothelial cells and the basal lamina. (**g**) Note flowing erythrocytes in anastomosing blood capillaries of cortical tissues prepared with IVCT (asterisks). Arrows: thymocytes. Arrowheads: epithelial reticulum cells. Bars=100 μm (**a**); 50, 20 μm (**b–f**).

DAB reaction of the luminal plasma faintly continued into the interstitium among thymocytes and reticulum cells (Fig. 3c, inset). The concentration of DAB reaction products gradually fell at a variable distance from the blood vessel (Fig. 3c). The different intensities of enzyme reactivity in a single section usually depended on the relative amount of actual enzymatic reaction. At 1 and 3 min, such enzyme reaction products were more widely found in the similar interstitium around thick blood vessels in the corticomedullary boundary areas (Fig. 3e–h). They appeared to be limitted at variable distances in the interstitium from the permeable blood vessels. At 10 min, they were more dif-

fusely detected mostly in the interstitium of cortical areas (Fig. 3i, j), and also detected in the intertitium of medullary areas (Fig. 3i, j). At 15 min, they were finally found to be distributed throughout all the interstitium of thymic tissues including both the cortex and medulla (Fig. 3k, l). It became obvious that the injected HRP diffused out from the blood vessels of corticomedullary areas, but not from blood capillaries in the outer cortex at a few minutes of time, as summarized in Table 1. In addition, at 30 min, HRP phagocytosis by many macrophages was seen throughout all the interstitium of the thymic tissues (Fig. 3m, n), which was accompanied by the rapid decrease of DAB reaction products in the interstitium of the cortex (Fig. 3m, n). However, they were still detected in the interstitium of the medulla, as shown in Figure 3n. Such different DAB reactivities in the medulla were probably related to both the flow rate of HRP from other areas and the rate of its removal from the medullary parenchyma. These DAB reaction products were not derived from endogenous peroxidase of the macrophages, because thymic macrophages were not heavily stained, like cells without HRP injection (Fig. 3a, b), which were later immunohistochemically confirmed by anti-HRP antibody (Fig. 5l, m).

It was previously unknown that leakage of HRP protein through blood vessels depends on not only molecular sizes or charges, but also on molecular concentrations in the blood vessels. At 3 min after their injection via left ventricles with lower concentrations of HRP, such as 10 and 25 mg/ml (Fig. 4c–f), a slight gradient of transudation into the interstitium through thick blood vessels was slightly seen in the thymus of living mice, depending on the HRP concentration. HRP enzyme reactivity was similarly detected in the interstitium around thick blood vessels in corticomedullary boundary areas and within some blood capillaries in the cortex (Fig. 4c–f). As schematically shown in Figure 2b, the cortical blood capillaries finally merged into postcapillary venules at the corticomedullary boundary and in the medulla. However, HRP enzyme reaction products were more heavily detected in the interstitium of inner cortical and medullary areas at higher concentrations of HRP, such as 50 and 100 mg/ml (Fig. 4g–j). A series of HRP injections with different concentrations revealed that the distribution of exogenous HRP was also dependent on the concentration of injected HRP, as summarized in Table 2. Therefore, no HRP was detected in the interstitium around blood capillaries in outer cortical areas at any concentration of injected HRP.

Immunolocalizations of HRP in paraffin sections of thymic tissues

To re-examine thymic tissues at higher resolution, both HE staining and HRP immunostaining were performed in serial paraffin sections of living mouse thymic tissues after short time intervals in the order of seconds to minutes, and were injected with a lower concentration of HRP (25 mg/ml) via the left ventricle. At 30 sec and 1 min (Fig. 5a–d), HRP immunoreactivity was detected only within blood vessels. At 3 and 10 min, however, it was weakly detected in the interstitium around blood vessels in corticomedullary boundary areas and within some blood capillaries in cortical areas (Fig. 5e–h). A striking feature was that immunostaining changes involved the inner cortex and especially the corticomedullary boundary of thymic tissues (Fig. 5f, h), as summarized in Table 3. Perivascular spaces of thick blood vessels were also immunopositive for HRP (Fig. 5f, h, insets). At 15 min, HRP immunoreactivity was more widely seen in the interstitium of the thymic cortex (Fig. 5i, j, arrows), but less than in blood vessels (Fig. 5i, j, arrowheads). At 30 min, it was a little more heavily detected in the interstitium of the medulla (Fig. 5l, m) as compared with the cortex, probably because there was a little more extravasation of HRP through venular walls, as summarized in Table 3. The permeability of HRP across the blood capillary walls was hardly seen in the outer cortical areas, as shown in Figures 5f and 5h. In addition, HRP phagocytosis by macrophages was clearly seen at 30 min after the HRP injection (Fig. 5m, double arrowheads), which was similar to that revealed by enzyme-histochemistry of HRP (Fig. 3m, n).

To more precisely examine HRP immunolocalization, double-immunofluoresconce staining of HRP and collagen type IV was perfomed for IVCT-prepared thymic tissues, which were prepared 3 min after HRP (25 mg/ml) injection. In corticomedullary boundary areas (Fig. 6a–f), HRP immunoreactivity was detected in the interstitium and perivascular spaces around thick blood vessels and also within blood vessels (Fig. 6a–f). In the cortical areas at 3 min after HRP injection, however, it was not detected in the interstitium around thick blood vessels, including blood capillaries (Fig. 6g–l).

Time-dependent detection of QDs in blood vessels of thymic tissues

The purposes to use QDs were to examine the transduction of larger molecular probes, QDs, through the blood vessel walls and also to visualize the blood flow condition rapidly changing in the order of seconds.

Mouse thymic tissues were prepared at 3, 10 and 30 sec after injection of QDs via left ventricles with IVCT. HE-staining micrographs (Fig. 7a, c, e) and fluorescence images (Fig. 7b, d, f) excited by UV wavelength definitely showed QD localization in blood capillaries and thick blood vessels, depending on the short-time intervals after QD injection, as summarized in Table 4. At 3 sec, QDs were partially detected in a few thick blood vessels in corticomedullary boundary areas (Fig. 7b, arrowheads), but not in others (Fig. 7b, arrows). At 10 sec, they were more clearly detected in thick blood vessels in boundary areas (Fig. 7d, arrowheads), but still not in thin blood capillaries (Fig. 7d, arrows). At 30 sec, they were most clearly found in all blood vessels, including thick blood vessels (Fig. 7f, arrowheads) and blood capillaries of thymic tissues (Fig.

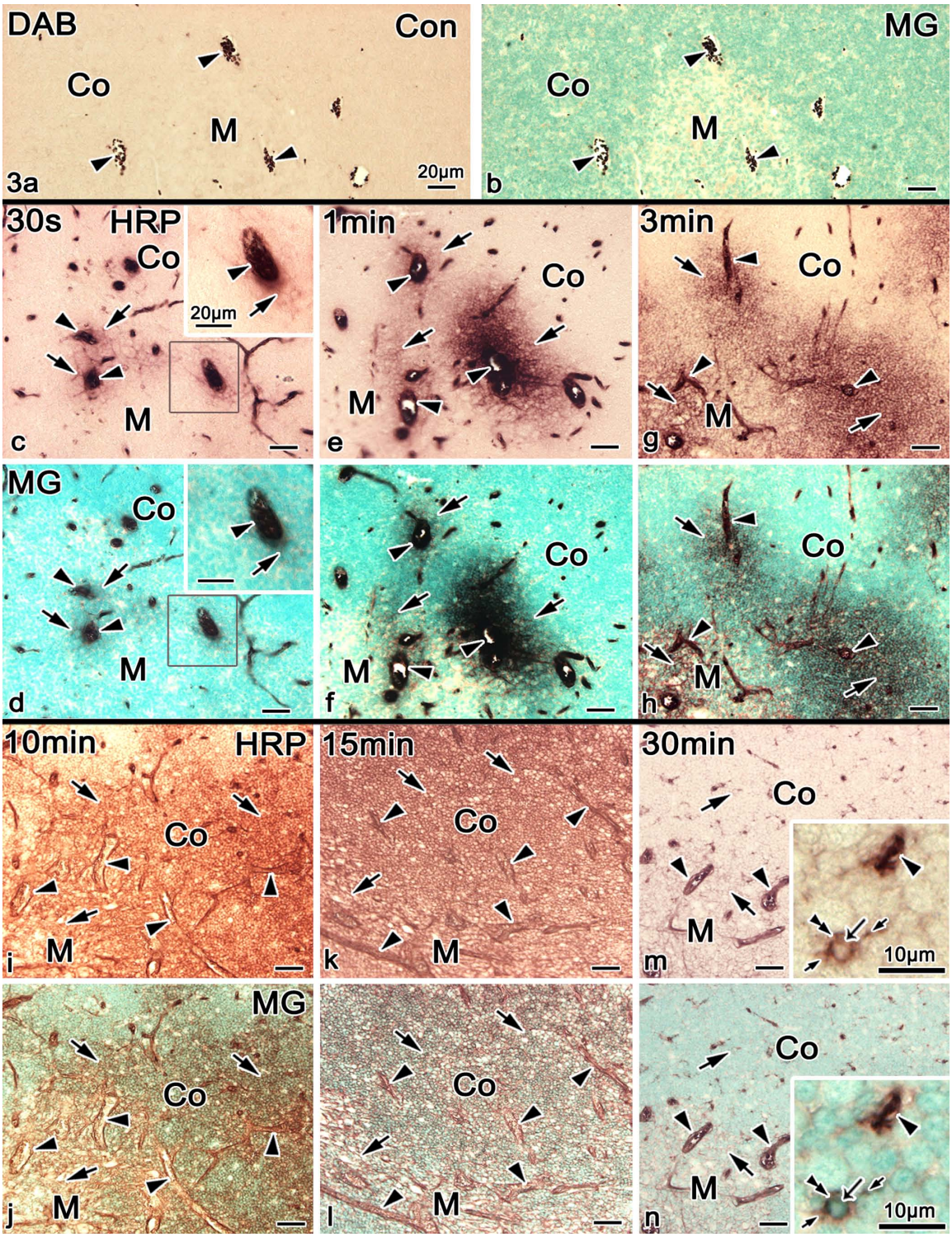

Fig. 3. Enzyme-histochemical images of DAB reaction of HRP in cryosections of mouse thymic tissues, which were injected with HRP (100 mg/ml) via left ventricles, and prepared after various time intervals by IVCT. (**a, b**) Control mice (Con) without HRP injection. Arrowheads: blood vessels. MG, methyl green staining. (**c, d**) At 30 sec, HRP reaction products are slightly detected in the interstitium around some thick blood vessels in corticomedullary boundary areas (arrows) and also within other blood vessels (arrowheads). (**e–h**) At 1 min and 3 min, they are more widely detected in the interstitium around thick blood vessels in corticomedullary boundary areas (arrows) and within some thick blood vessels in both cortical and medullary areas (arrowheads). (**i, j**) At 10 min, they are diffusely detected in all the interstitium of cortical and medullary areas (arrows). (**k, l**) At 15 min, they are uniformly distributed throughout all the interstitium of thymic tissues (arrows) in addition to perivascular spaces of blood vessels (arrowheads). (**m, n**) At 30 min, HRP phagocytosis by macrophages (double arrowheads) is seen to be scattered, which is accompanied by the decrease of DAB reaction intensity in all the interstitial matrix. Arrowhead: blood vessel. Long arrow: nucleus. Short arrow: process. Co, cortex. M, medulla. Bars=20 μm.

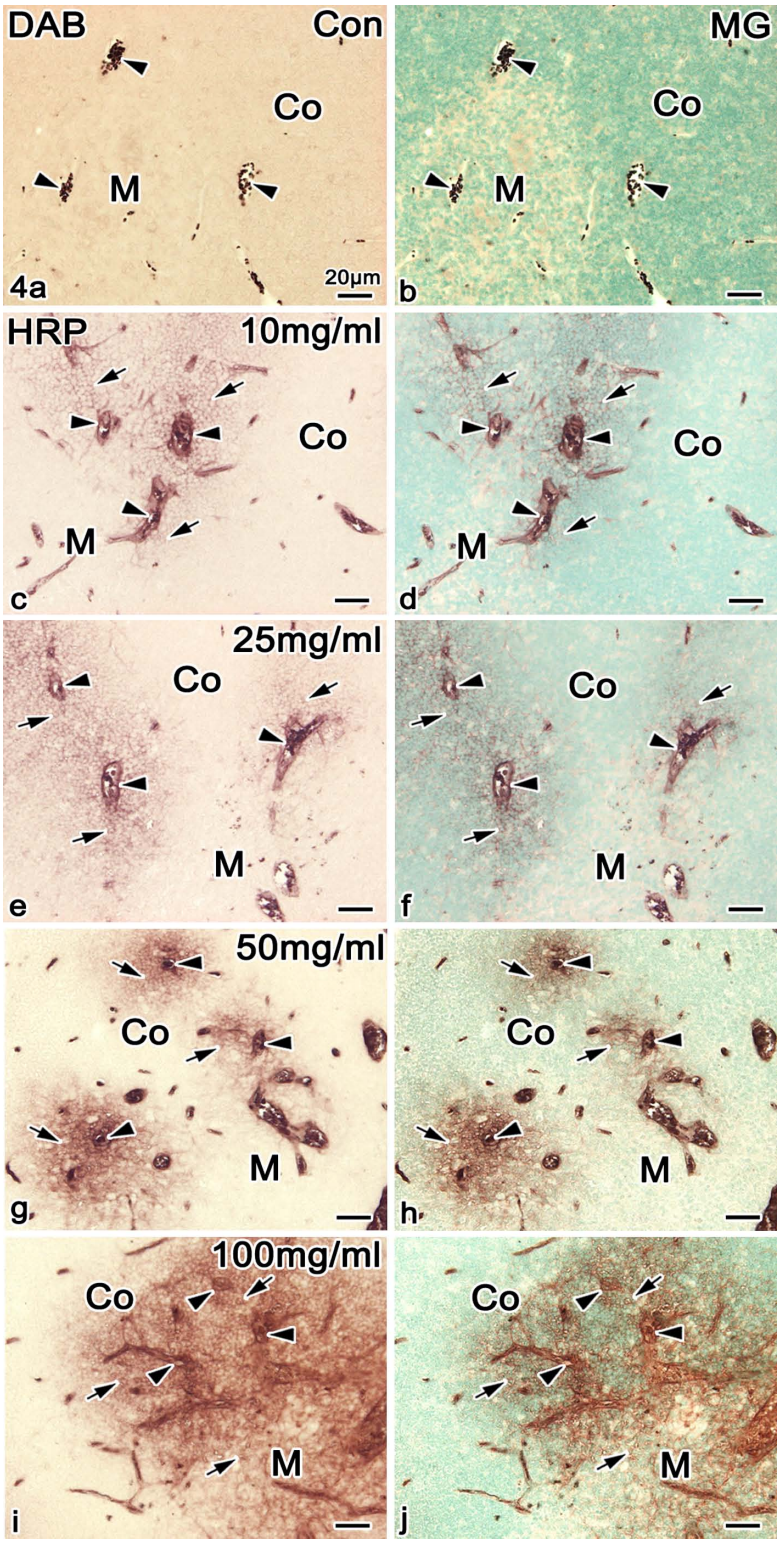

Fig. 4. Enzyme-histochemical images of DAB reaction of HRP in cryosections of mouse thymic tissues, which were injected with various concentrations of HRP [10 (**c, d**), 25 (**e, f**), 50 (**g, h**) and 100 mg/ml (**i, j**)] via left ventricles, and prepared at 3 min after HRP injection by IVCT. (**a, b**) Control mice (Con) without HRP injection. MG, methyl green staining. (**c–j**) HRP-enzyme reactivities are variously detected in the interstitium (arrows) around some blood vessels in corticomedullary boundary areas and other thick blood vessels of the medulla, depending on the HRP concentration, but they are also found within blood vessels (arrowheads) in addition to tiny blood capillaries. Co, cortex. M, medulla. Bars=20 μm.

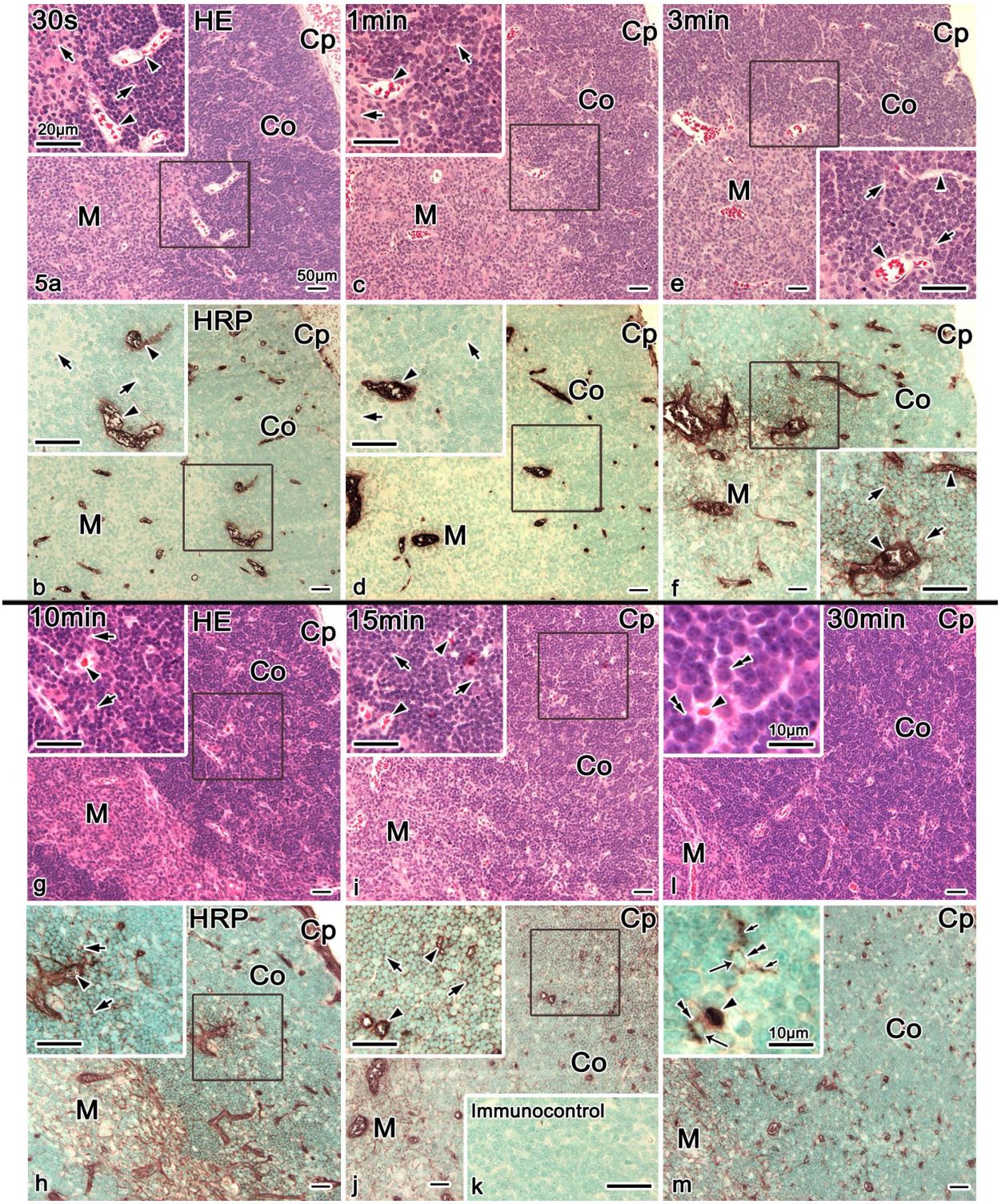

Fig. 5. Light microscopic images of hematoxylin-eosin (HE) staining (**a, c, e, g, i, l**) and HRP immunostaining (**b, d, f, h, j, m**) in serial paraffin sections of mouse thymic tissues, which were injected with a lower concentration of HRP (25 mg/ml) via left ventricles, and prepared after various time intervals by IVCT. (**a–d**) At 30 sec and 1 min, HRP immunoreactivity is detected only within blood vessels (arrowheads), not in the interstitium around them. (**e, f**) However, at 3 min, it is weakly detected in the interstitium (arrows) around blood vessels in corticomedullary boundary areas and within some thick blood vessels (arrowheads). (**g, h**) At 10 min, HRP immunoreactivity is also detected in the interstitium (arrows) around blood vessels in corticomedullary boundary areas and within thick blood vessels (arrowhead). (**i, j**) At 15 min, it is more widely seen in the interstitium (arrows), as compared with blood vessels (arrowheads). (**k**) Immunocontrol. (**l, m**) In addition, HRP phagocytosis by macrophages (double arrowheads) is seen at 30 min after HRP injection. Arrowheads: blood vessels. Long arrows: nuclei. Short arrows: processes. Cp, capsule. Co, cortex. M, medulla. Bars=50 μm; insets, 20 μm.

Table 1. *Semi-quantitative comparison of relative HRP enzyme reactivity, as shown in Figure 3, in thymic tissues of cryosections at various time intervals after HRP (100 mg/ml) injection*

		Normal	HRP injection (100 mg/ml) times via left ventricles					
			30 s	1 min	3 min	10 min	15 min	30 min
Blood vessels (15–30 μm) in corticomedullary boundary areas	Inside of vessels	–	+++	+++	+++	++	++	+
	Interstitium around vessels	–	+	++	++	+++	++	±
Blood capillaries (~10 μm) in outer cortical areas	Inside of capillaries	–	+++	+++	+++	++	++	+
	Interstitium around capillaries	–	–	–	±	+	++	±
Phagocytosis of macrophages	Cortical areas	–	–	–	–	–	+	+++
	Medullary areas	–	–	–	–	–	+	+++

(+++) Strong enzyme reaction, (++) Moderately positive, (+) Slightly positive, (±) Unclear, (–) Negative.

Table 2. *Semi-quantitative comparison of relative HRP enzyme reactivity, as shown in Figure 4, in thymic tissues of cryosections, depending on different concentrations (10 mg/ml, 25 mg/ml, 50 mg/ml, 100 mg/ml) at 3 min after HRP injection*

		Normal	Injected HRP concentrations			
			10 mg/ml	25 mg/ml	50 mg/ml	100 mg/ml
Blood vessels (15–30 μm) in corticomedullary boundary areas	Inside of vessels	–	+	+	++	++
	Interstitium around vessels	–	±	+	++	++
Blood capillaries (~10 μm) in outer cortical areas	Inside of capillaries	–	+	+	++	++
	Interstitium around capillaries	–	–	–	–	±

(++) Moderately positive, (+) Slightly positive, (±) Unclear, (–) Negative.

Table 3. *Semi-quantitative comparison of relative HRP immunoreactivity, as shown in Figure 5, in different areas of living mouse thymic tissues after HRP (25 mg/ml) injection on paraffin-embedded sections*

		Normal	HRP injection (25 mg/ml) times via left ventricles					
			30 s	1 min	3 min	10 min	15 min	30 min
Blood vessels (15–30 μm) in corticomedullary boundary areas	Inside of vessels	–	+	+	+	+	+	+
	Interstitium around vessels	–	–	–	+	++	++	+
Blood capillaries (~10 μm) in outer cortical areas	Inside of capillaries	–	+	+	+	+	+	+
	Interstitium around capillaries	–	–	–	–	–	+	±
Phagocytosis of macrophages	Cortical areas	–	–	–	–	–	+	++
	Medullary areas	–	–	–	–	–	+	++

(++) Moderately immunopositive, (+) Slightly immunopositive, (±) Unclear, (–) Negative.

7f, arrows), similarly showing that QDs did not enter the thymic interstitium, which was compatible with other organs, such as the kidneys [36].

To reconfirm the blood circulation routes of blood vessels and also the HRP permeability of various vessel sizes at corticomedullary boundary areas at the same time, we checked the colocalization of both QDs and HRP in some serial sections by fluorescence or light microscopy (Fig. 8). At 10 sec after the mixed QD and HRP injection (Fig. 8a–c), both were exclusively localized within blood vessels of the cortex and medulla. However, at 15–30 sec after a similar injection (Fig. 8d–i), only HRP had leaked out into the interstitium around some thick blood vessels in corticomedullary boundary areas, not in the cortex. In contrast, other QDs were still localized within blood vessels. When we carefully examined the tissue specimens at 15 or

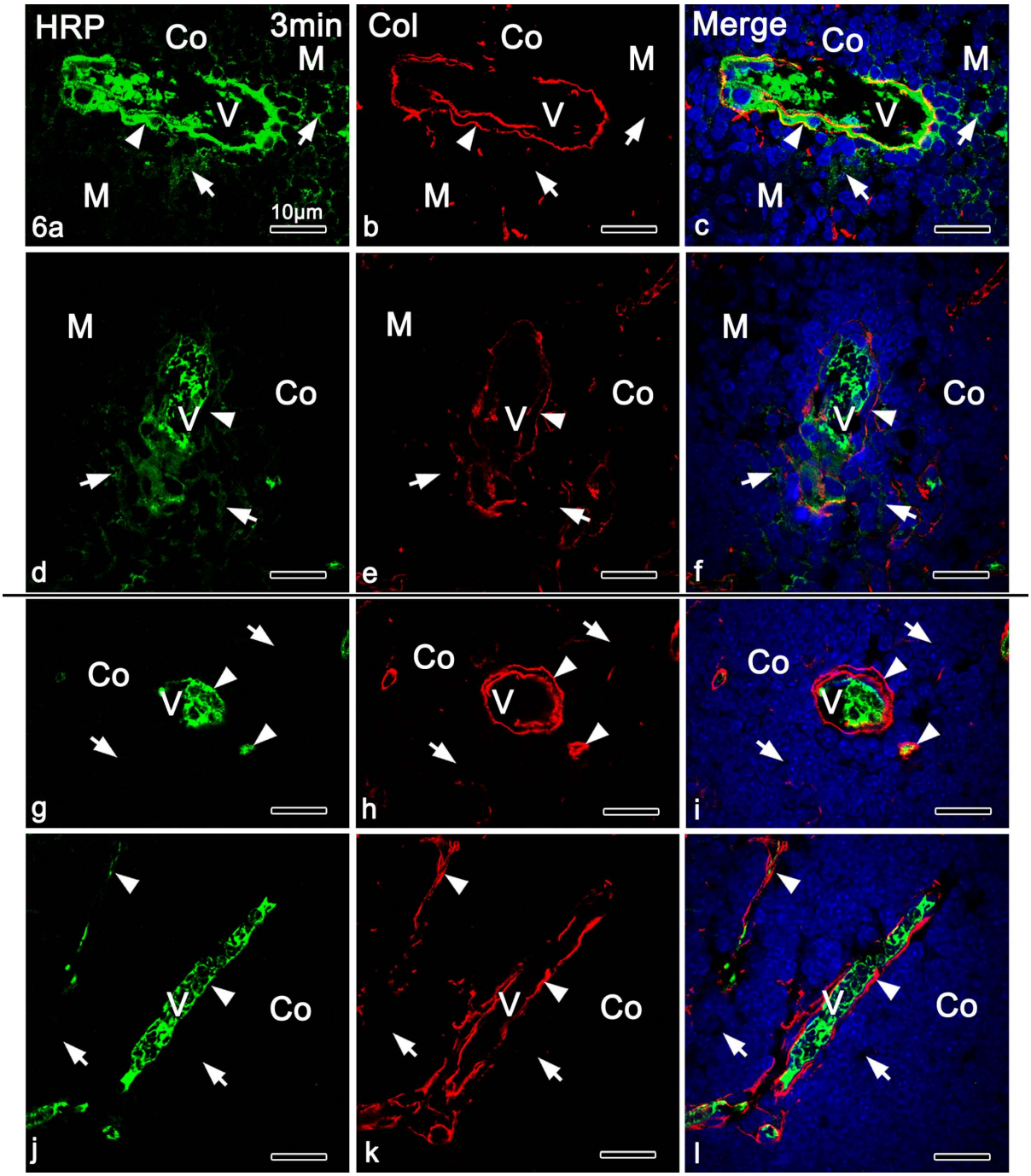

Fig. 6. Double-immunofluorescence micrographs of HRP (**a, d, g, j**) and collagen type IV (**b, e, h, k**), including merged images (**c, f, i, l**), are shown in cryosections of IVCT-prepared thymic tissues 3 min after HRP (25 mg/ml) injection, indicating the corticomedullary boundary (**a–f**) and cortical areas (**g–l**). HRP immunoreactivity is detected in the interstitium around some thick blood vessels (V) of corticomedullary boundary areas (arrows in **a–f**) and within blood vessels (arrowheads in **a–f**), but it is not seen in the interstitiumin around blood vessels in cortical areas (arrows in **g–l**). Some perivascular spaces are clearly seen as double lines with immunostaining for collagen type IV (**b, e, h, k**) and HRP is immunolocalized only in blood vessels of the cortex (arrowheads in **g–l**). V: blood vessels. Co, cortex. M, medulla. Bars=10 μm.

30 sec after the injection, we sometimes found much heavier leakage of HRP through thick blood vessels than smaller vessels in corticomedullary boundary areas (Fig. 8e, h). In summary, QDs flowing in thymic blood vessels did not leak out into the interstitium of thymic tissues in the order of seconds, as reported before [36].

Demonstration of HRP phagocytosis by macrophages

Cryosections of mouse thymic cortical areas, which were injected with HRP (100 mg/ml) via left ventricles and prepared at 30 min by IVCT, were examined to show double-immunofluorescence staining for HRP (Fig. 9a, c) and Iba1, a macrophage marker (Fig. 9b, c), together with

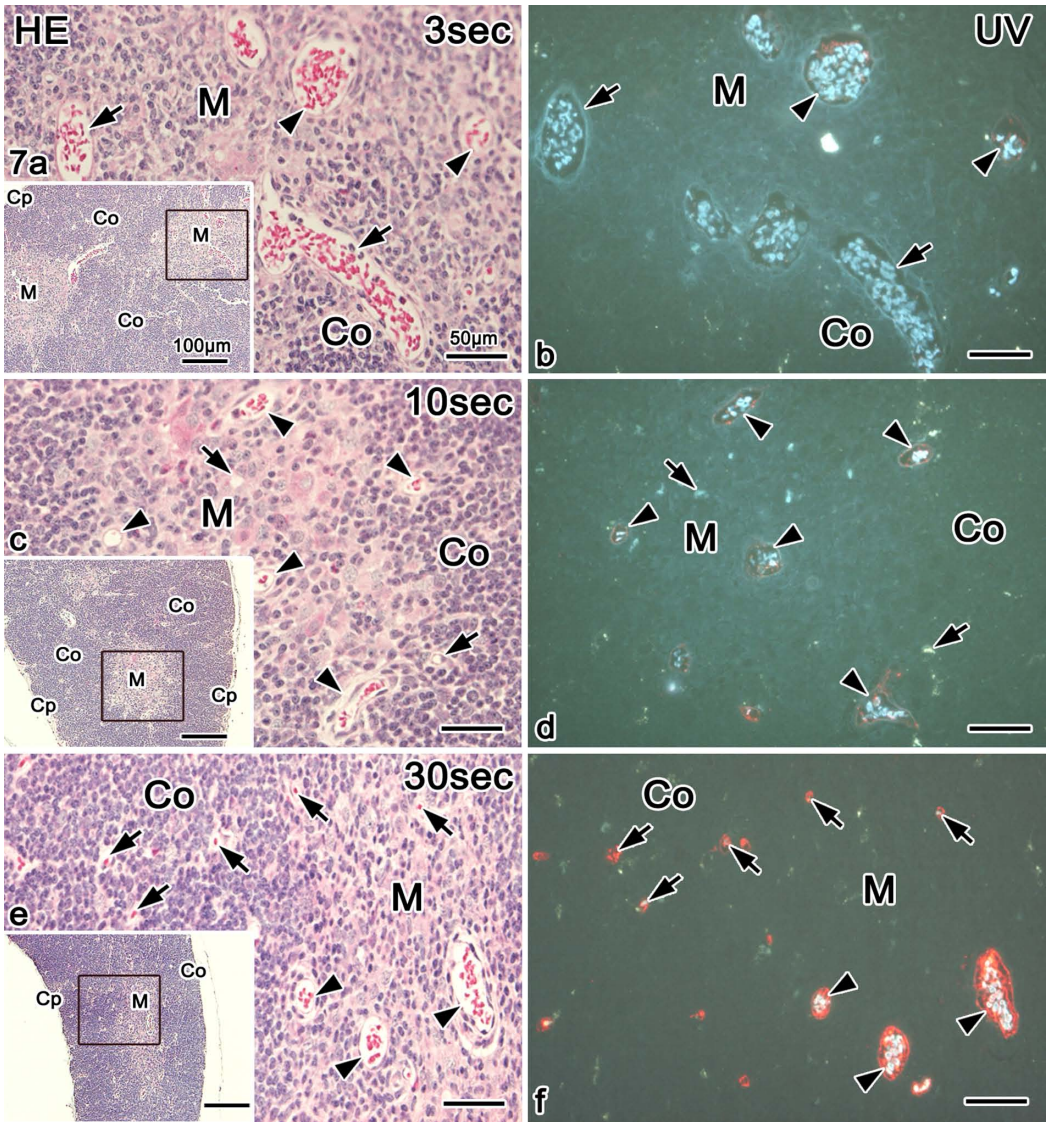

Fig. 7. Light micrographs of paraffin sections of mouse thymic tissues at 3 (**a, b**), 10 (**c, d**) and 30 sec (**e, f**) after QD injections via left ventricles, prepared with IVCT. Both hematoxylin-eosin staining (HE; **a, c, e**) and red fluorescence signals (UV; **b, d, f**) emitted by ultraviolet wavelength were checked in serial tissue sections. (**a, b**) At 3 sec, QDs are slightly detected in small numbers of thick blood vessels (arrowheads) in corticomedullary boundary areas, but not in other blood vessels (arrows), including blood capillaries. (**c, d**) At 10 sec, they are more widely detected in the blood vessels in corticomedullary boundary areas (arrowheads), but are not yet seen in blood capillaries (arrows). (**e, f**) At 30 sec, they are seen in all the thick blood vessels (arrowheads), including blood capillaries (arrows), of the thymic tissues. Co, cortex. M, medulla. Bars=50 μm; inset, 100 μm.

Table 4. *Semi-quantitative comparison of relative QD localizations, as shown in Figure 7, in blood vessels of different areas of thymic tissues after QD injection on paraffin-embedded sections*

		Time intervals after QD injection via left ventricles		
		3 s	10 s	30 s
Blood vessels (15–30 μm) in corticomedullary boundary areas	Inside of vessels	+	++	+++
	Interstitium around vessels	–	–	–
Blood capillaries (~10 μm) in outer cortical areas	Inside of capillaries	–	+	++
	Interstitium around capillaries	–	–	–

(+++) Strongly positive, (++) Moderately positive, (+) Slightly positive, (–) Negative.

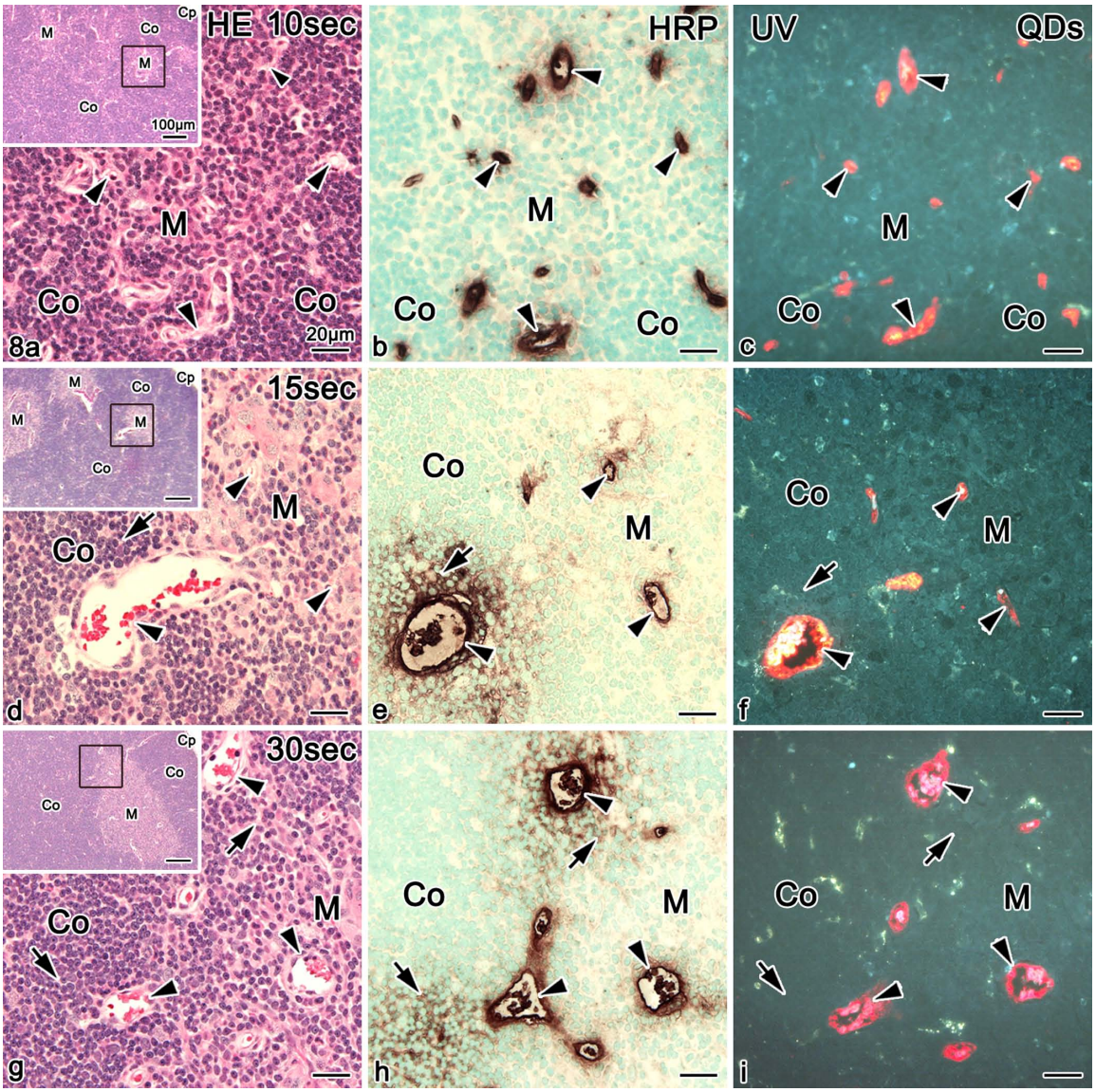

Fig. 8. Light micrographs of colocalization of QDs and HRP in serial paraffin sections by fluorescence or light microscopy. At 10 sec after the mixed QD and HRP injection, both are seen in blood vessels (arrowheads in **b, c**). At 15–30 sec, HRP has definitely leaked out into the interstitium around some thick blood vessels in the corticomedullary boundary areas (arrows in **e, h**), not in the cortex, but the QDs are still localized in blood vessels (arrowheads in **f, i**). Co, cortex. M, medulla. **a, d, g**: HE staining. **b, e, h**: immunostaining for HRP. **c, f, i**: fluorescent QDs. Bars=20 μm.

DAPI staining (Fig. 9c). The red fluorescence signals of Iba1 were mainly detected in the cytoplasm of macrophages, and HRP immunostaining was also seen in macrophages (Fig. 9c, double arrowheads). HRP immunofluorescence was still detected in blood vessels 30 min after HRP injection (Fig. 9a, c, arrowheads), in addition to some local interstitial areas (Fig. 9a, c, arrows).

IV. Discussion

Merits of IVCT for demonstration of HRP

The main feature of IVCT presented in this study was to obtain tissue specimens of living animal organs, which can strictly capture their dynamic circulation states including cells and tissues, as already discussed in detail [27]. It is well known that conventional immunohistochemical techniques have some problems with molecular diffusion artifacts and antigen masking for the detection of soluble components in living animal organs. In contrast, the IVCT has various technical merits, including the prevention of tissue shrinkage or diffusion artifacts, a natural antigen-retrieval effect, and time-dependent analyses in the order of seconds. Therefore, it has been often used to analyze the immunolocalization of soluble proteins in cells and tissues of living aminal organs under various hemodynamic conditions [27]. As compared with previons studies of molecular movement in the thymic interstitium for immunology, such as antigen presentation in functional thymic tissues [17], the present study showed small molecular HRP with dose- and time-dependent leakage through different thymic blood

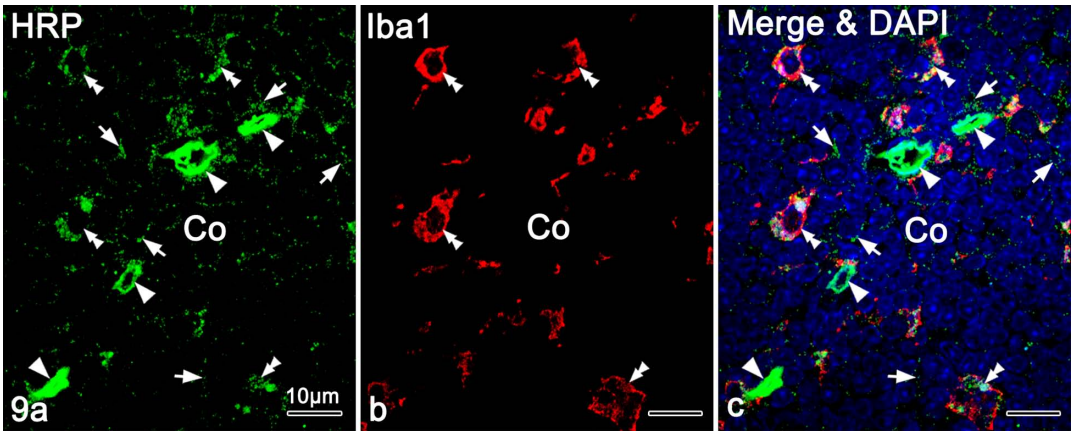

Fig. 9. Immunofluorescence micrographs of cryosections of thymic cortical areas at 30 min after HRP (100 mg/ml) injection via left ventricles of living mice, prepared by IVCT. Double-immunofluorescence staining for HRP (**a, c**, green) and ionized calcium-binding adapter molecule 1 (Iba1) (**b, c**, red) with nuclear DAPI staining (blue) show their colocalization in almost all macrophages. Iba1 immunofluorescence shows the macrophages of thymic tissues (**b, c**, double arrowheads), which contain HRP in their cytoplasm (**a, c**, double arrowheads). HRP immunostaining is still detected within the blood vessels (**a, c**, arrowheads) and some areas of the cortical interstitium among compact thymocytes (**a, c**, arrows). Co, cortex. Bars=10 μm.

vessels, because of the high time-resolution of IVCT for dynamic functional structures [36]. Although the IVCT is a cryofixation method, which is not designed for time-lapse imaging, the present study also indicates that it is useful to examine the dynamically changing flux of extrinsic soluble HRP proteins in the thymic tissues. The IVCT was also found to be used for both enzyme-histochemical or immunohistochemical studies of soluble HRP circulation, as shown in Figures 3–5, and would be helpful for other enzyme-histochemical analyses due to the remaining high sensitivity of cryofixed enzyme reactions.

Permeability of HRP or BSA through different blood vessels

It is well known that the animal thymus has a special vascular complex, conventionally termed the blood–thymus barrier [3, 7, 15, 17, 29, 30], as an initial exposure site of lymphocytes to circulating antigens. The blood–thymus barrier has been assumed to be a reliable structure in the anatomical and functional sense, but foreign antigens can probably permeate its barrier under certain conditions. It has been also reported to consist of capillary endothelial cells, basal lamina of endothelium, perivascular spaces, basal lamina of epithelial reticulum cells and finally epithelial reticulum cells themselves. A previous experiment using ultrastructural tracers of different molecular weights demonstrated that immunological lymphoid cells in the thymic cortex were usually protected from circulating antigenic molecules in contrast with those of the medulla [29]. The interstitial tissues with augmented permeability of antigen proteins under some conditions *in vivo* would increase the accessibility of thymocytes to blood-derived molecules. However, based on the experiment with BSA of various concentrations, as performed previously using the living mouse thymic tissues [3], we found that the injected BSA was time-dependently distributed throughout the thymic interstitium in hours to days, leaking from thick blood vessels at the corticomedullary boundary, but not from blood capillaries in outer cortical areas. In the present study, we have also revealed the similar localization of HRP protein in the thymic interstitium of living mice in a few minutes, indicating the easy leakage of small molecular HRP into corticomedullary boundary areas, depending on the time after HRP injection and its concentration, as shown in Figures 3–5. Therefore, these findings also supported the partial existence of a functional blood–thymus barrier, especially along blood capillaries of the outer cortex, although the molecular permeability of thick blood vessels, including some arterioles, in corticomedullary boundary areas was higher than that in the outer cortex, as already discussed [4, 15, 30]. In contrast, the thymic medulla contains leaky blood vessels, namely postcapillary venules. The time- and concentration-dependent localization of antigenic HRP proteins might be helpful for other immunohistochemical analyses of native thymic structures tissues with various interstitial fluid pressures and also determination of the immunological system *in vivo*.

Different states of blood-thymus barriers

In the case of QD injection with a high molecular complex, we did not find leakage of QD probes through any blood vessels of thymic tissues in the order of seconds, as shown in Figures 7 and 8. Our findings definitely showed the blood flow route from thick arterioles at the corticomedullary boundary at 3 sec, and then to thin blood capillaries in the inner cortex, as schematically summarized in Figure 2b. In addition, other reports have already demonstrated that transudation into thymic interstitial matrices depended on the molecular weight of the administered substances [4, 7, 13, 16, 17, 23, 29, 31]. The distribution of injected HRP of low molecular weight presented in this study seems to be additionally related to the vascular structures in the thymic cortex, because larger intrinsic IgA and IgM immunostaining intensities were less detected in the outer cortex in comparison with both extrinsic BSA and

mouse original albumin, as already discussed [3]. Therefore, it is concluded that an incomplete blood–thymus barrier in the corticomedullary boundary areas usually contributes to such different morphofunctional data of thymic tissues of living mice, which was directly revealed by IVCT-FS, probably reflecting their living state.

Demonstration of native blood flow routes

In addition, rapid QD distribution in the order of seconds was also visualized in the living mouse thymus with IVCT-FS, reflecting the *in vivo* blood flow condition, as reported previously [36]. Following the scheme of blood vessels (Fig. 2b), they formed branching and anastomosing loops in outermost regions of the cortical area. At the junction of the cortex and medulla, arterioles usually run upward to the surface capsule, continuing into blood capillaries within a short distance under the capsule, and then blood capillaries return as postcapillary venules to medullary thick veins (Fig. 2b). In corticomedullary boundary areas, arteries branch into arterioles, from which anastomosing blood capillaries break off into the inner cortex. As shown in Figures 7 and 8, QDs flowing in blood vessels did not leak out into the interstitium of thymic tissues in the order of seconds, indicating no transudation of QDs of larger molecular size, as discussed previously [36].

Phagocytosis of leaked HRP into macrophages

In the thymus, as shown in Figure 9, macrophages around the blood vessels actively phagocytized the permeated HRP. The permeability of the vessels in the thymus is known to be relatively low, as compared with that of blood vessels in other lymphatic tissues. Four subpopulations of mouse thymic macrophages have already been identified, including dendritic macrophages, plate-shaped macrophages, small oval macrophages, and $ED1^{+}$-thymic macrophages [20]. Each subpopulation has different functions in the outer or inner cortex and the medulla. The HRP immunostaining intensity later decreased in the interstitium of the thymic cortex in comparison with the inside of blood vessels, as shown in Figures 3m and 5m. Such phagocytotic functions of macrophages within 30 min might change the average molecular concentrations of HRP in the thymic interstitium, depending on the time course of flowing HRP molecules. Moreover, the phagocytosis of HRP into macrophages could induce their expression of specific antigens, probably resulting in the common positive or negative immunoreaction pathway in other thymic cells. Therefore, in a future study, the IVCT will be additionally used to clarify T-cell differentiation at various sites of thymic tissues, probably depending on the dynamic diffusion of various serum components in their microenvironment. A further experiment at an electron microscopic level will be also necessary to directly examine the HRP penetration of blood vessels and phagocytotic macrophages of living mice, which could be prepared by IVCT.

V. Acknowledgments

The authors thank Dr. T. Jin, Laboratory for Nano-Bio Probes, RIKEN Quantitative Biology Center, Suita City, Osaka, Japan, for the gift of glutathione-coated quantum dots.

VI. References

1. Bai, Y., Ohno, N., Terada, N., Saitoh, S., Nakazawa, T., Nakamura, N., Katoh, R. and Ohno, S. (2009) Immunolocalization of serum proteins in xenografted mouse model of human tumor cells by various cryotechniques. *Histol. Histopathol.* 24; 717–728.
2. Bai, Y., Wu, B., Terada, N., Ohno, N., Saitoh, S., Saitoh, Y. and Ohno, S. (2011) Histological study and LYVE-1 immunolocalization of mouse mesenteric lymph nodes with “in vivo cryotechnique”. *Acta Histochem. Cytochem.* 44; 81–90.
3. Bai, Y., Wu, B., Terada, N., Saitoh, Y., Ohno, N., Saitoh, S. and Ohno, S. (2012) Immunohistochemical analysis of various serum proteins in living mouse thymus with “in vivo cryotechnique”. *Med. Mol. Morphol.* 45; 129–139.
4. Drumea-Mirancea, M., Wessels, J. T., Müller, C. A., Essl, M., Eble, J. A., Tolosa, E., Koch, M., Reinhardt, D. P., Sixt, M., Sorokin, L., Stierhof, Y., Schwarz, H. and Klein, G. (2006) Characterization of a conduit system containing laminin-5 in the human thymus: a potential transport system for small molecules. *J. Cell Sci.* 119; 1396–1405.
5. Elmore, S. A. (2006) Enhanced histopathology of the thymus. *Toxicol. Pathol.* 34; 656–665.
6. Graham, R. C. Jr. and Karnovsky, M. J. (1966) The early stages of absorption of injected horseradish peroxidase in the proximal tubules of mouse kidney: ultrastructural cytochemistry by a new technique. *J. Histochem. Cytochem.* 14; 291–302.
7. Green, I. and Bloch, K. (1963) Uptake of particulate matter within the thymus of adult and new-born mice. *Nature* 200; 1099–1101.
8. Henry, L., Durrant. T. E. and Anderson, G. (1992) Pericapillary collagen in the human thymus: implications for the concept of the ‘blood-thymus’ barrier. *J. Anat.* 181; 39–46.
9. Hopwood, D. (1969) Fixatives and fixation: a review. *Histochem. J.* 1; 323–360.
10. Hopwood, D. (1985) Cell and tissue fixation, 1972–1982. *Histochem. J.* 17; 389–442.
11. Ito, T. and Hoshino, T. (1966) Light and electron microscopic observations on the vascular pattern of the thymus of the mouse. *Arch. Histol. Jpn.* 27; 351–361.
12. Jin, T., Fujii, F., Komai, Y., Seki, J., Seiyama, A. and Yoshioka, Y. (2008) Preparation and characterization of highly fluorescent, glutathione-coated near infrared quantum dots for in vivo fluorescence imaging. *Int. J. Mol. Sci.* 9; 2044–2061.
13. Kato, S. (1997) Thymic microvascular system. *Microsc. Res. Tech.* 38; 287–299.
14. Kazuta, Y. (1994) An Atlas of the Experimental Animal Technology. Adthree Publishing Co. Ltd, Tokyo, Japan, p. 13.
15. Kendall, M. D. (1991) Functional anatomy of the thymic microenvironment. *J. Anat.* 177; 1–29.
16. Kyewski, B. A., Fathman, C. and Kaplan, H. (1984) Intrathymic presentation of circulating non-major histocompatibility complex antigens. *Nature* 308; 196–199.
17. Kyewski, B. A., Fathman, C. G. and Rouse, R. V. (1986) Intrathymic presentation of circulating non-MHC antigens by medullary dendritic cells: an antigen-dependent microenvironment for T cell differentiation. *J. Exp. Med.* 163; 231–246.

18. Ladi, E., Yin, X., Chtanova, T. and Robey, E. A. (2006) Thymic microenvironments for T cell differentiation and selection. *Nat. Immunol.* 7; 338–343.
19. Lind, E. F., Prockop, S. E., Porritt, H. E. and Petrie, H. T. (2001) Mapping precursor movement through the postnatal thymus reveals specific microenvironments supporting defined stages of early lymphoid development. *J. Exp. Med.* 194; 127–134.
20. Liu, L. T., Lang, Z. F., Li, Y., Zhu, Y. J., Zhang, J. T., Guo, S. F., Wang, J. X., Wang, H. W. and Xu, Y. D. (2013) Composition and characteristics of distinct macrophage subpopulations in the mouse thymus. *Mol. Med. Rep.* 7; 1850–1854.
21. Marshall, A. H. and White, R. G. (1961) The immunological reactivity of the thymus. *Br. J. Exp. Pathol.* 42; 379–385.
22. Mason, D. Y. and Biberfeld, P. (1980) Technical aspects of lymphoma immunohistology. *J. Histochem. Cytochem.* 28; 731–745.
23. Müller, S. M., Stolt, C. C., Terszowski, G., Blum, C., Amagai, T., Kessaris, N., Iannarelli, P., Richardson, W. D., Wegner, M. and Rodewald, H. (2008) Neural crest origin of perivascular mesenchyme in the adult thymus. *J. Immunol.* 180; 5344–5351.
24. Ohno, N., Terada, N. and Ohno, S. (2006) Histochemical analyses of living mouse liver under different hemodynamic conditions by "in vivo cryotechnique." *Histochem. Cell Biol.* 126; 389–398.
25. Ohno, N., Terada, N., Bai, Y., Saitoh, S., Nakazawa, T., Nakamura, N., Naito, I., Fujii, Y., Katoh, R. and Ohno, S. (2008) Application of cryobiopsy to morphological and immunohistochemical analyses of xenografted human lung cancer tissues and functional blood vessels. *Cancer* 113; 1068–1079.
26. Ohno, S., Terada, N., Fujii, Y., Ueda, H. and Takayama, I. (1996) Dynamic structure of glomerular capillary loop as revealed by an in vivo cryotechnique. *Virchows Arch.* 427; 519–527.
27. Ohno, S., Terada, N., Ohno, N., Saitoh, S., Saitoh, Y. and Fujii, Y. (2010) Significance of 'in vivo cryotechnique' for morphofunctional analyses of living animal organs. *J. Electron Microsc.* 59; 395–408.
28. Pearse, G. (2006) Normal structure, function and histology of the thymus. *Toxicol. Pathol.* 34; 504–514.
29. Raviola, E. and Karnovsky, M. J. (1972) Evidence for a blood–thymus barrier using electron-opaque tracers. *J. Exp. Med.* 136; 466–498.
30. Roberts, R. L. and Sandra, A. (1994) Transport of transferrin across the blood-thymus barrier in young rats. *Tissue Cell* 26; 757–766.
31. Sainte-Marie, G. (1963) Antigen penetration into the thymus. *J. Immunol.* 91; 840–845.
32. Saitoh, S., Terada, N., Ohno, N. and Ohno, S. (2008) Distribution of immunoglobulin-producing cells in immunized mouse spleens revealed with "in vivo cryotechnique". *J. Immunol. Methods* 29; 114–126.
33. Shi, L., Terada, N., Saitoh, Y., Saitoh, S. and Ohno, S. (2011) Immunohistochemical distribution of serum proteins in living mouse heart with in vivo cryotechnique. *Acta Histochem. Cytochem.* 44; 61–72.
34. Shimo, S., Saitoh, S., Terada, N., Ohno, N., Saitoh, Y. and Ohno, S. (2010) Immunohistochemical detection of soluble immunoglobulins in living mouse small intestines using an in vivo cryotechnique. *J. Immunol. Methods* 361; 64–74.
35. Terada, N., Ohno, N., Li, Z., Fujii, Y., Baba, T. and Ohno, S. (2006) Application of in vivo cryotechnique to the examination of cell and tissues in living animal organs. *Histol. Histopathol.* 21; 265–272.
36. Terada, N., Saitoh, Y., Saitoh, S., Ohno, N., Jin, T. and Ohno, S. (2010) Visualization of microvascular blood flow in mouse kidney and spleen by quantum dot injection with "in vivo cryotechnique". *Microvasc. Res.* 80; 491–498.
37. Tiwari, D. K., Tanaka, S., Inouye, Y., Yoshizawa, K., Watanabe, T. M. and Jin, T. (2009) Synthesis and characterization of anti-HER2 antibody conjugated CdSe/CdZnS quantum dots for fluorescence imaging of breast cancer cells. *Sensors* 9; 9332–9364.